Spindle–F-actin interactions in mitotic spindles in an intact vertebrate epithelium

Angela M. Kita[a,b,†], Zachary T. Swider[a,b,†], Ivan Erofeev[c], Mary C. Halloran[d,e], Andrew B. Goryachev[c], and William M. Bement[a,b,d,*]

[a]Cellular and Molecular Biology Graduate Program, [b]Laboratory of Cell and Molecular Biology, [d]Department of Integrative Biology, and [e]Department of Neuroscience, University of Wisconsin–Madison, Madison, WI 53706; [c]Centre for Synthetic and Systems Biology, University of Edinburgh, Edinburgh EH9 3JD, United Kingdom

ABSTRACT Mitotic spindles are well known to be assembled from and dependent on microtubules. In contrast, whether actin filaments (F-actin) are required for or are even present in mitotic spindles has long been controversial. Here we have developed improved methods for simultaneously preserving F-actin and microtubules in fixed samples and exploited them to demonstrate that F-actin is indeed associated with mitotic spindles in intact *Xenopus laevis* embryonic epithelia. We also find that there is an "F-actin cycle," in which the distribution and organization of spindle F-actin changes over the course of the cell cycle. Live imaging using a probe for F-actin reveals that at least two pools of F-actin are associated with mitotic spindles: a relatively stable internal network of cables that moves in concert with and appears to be linked to spindles, and F-actin "fingers" that rapidly extend from the cell cortex toward the spindle and make transient contact with the spindle poles. We conclude that there is a robust endoplasmic F-actin network in normal vertebrate epithelial cells and that this network is also a component of mitotic spindles. More broadly, we conclude that there is far more internal F-actin in epithelial cells than is commonly believed.

INTRODUCTION

The mitotic spindle of animal cells is arguably one of the most important structures found in eukaryotes: it not only partitions the chromosomes, it also partitions the centrosomes and ensures that cytokinesis occurs at the right place and time. Accordingly, the mitotic spindle has been the subject of long and intense scrutiny. Since its discovery in the 1800s, thousands of investigations have been performed to characterize its morphology, regulation, dynamics, and composition. As a consequence, we now possess an enormous amount of information concerning mitotic spindles in animal cells including detailed parts lists for the spindle as a whole (Nousiainen *et al.*, 2006), and for different spindle substructures

(e.g., Skop *et al.*, 2004; Kimura *et al.*, 2014). Moreover, our understanding of the roles played by these parts has reached a point where important features of spindle behavior can be successfully captured by mathematical modeling (e.g., Loughlin *et al.*, 2011; Magidson *et al.*, 2015).

And yet, in spite of this wealth of information, an old but important question has not yet been satisfactorily answered: What role, if any, does F-actin play in mitotic spindles (Sandquist *et al.*, 2011)? The consensus is that if F-actin influences mitotic spindles at all it does so by indirect anchoring of astral microtubules at the cortex that, in some cell types, permits proper spindle positioning (e.g., Théry *et al.*, 2005; Toyoshima and Nishida, 2007) or spindle pole separation (e.g., Rosenblatt *et al.*, 2004). Other potential roles for F-actin are largely discounted for one simple reason: there is little evidence that F-actin associates with the mitotic spindle in animal cells. That is, although early reports described spindle-associated F-actin in several different mammalian cell types (Gawadi, 1971; Sanger, 1975; Cande *et al.*, 1977; Schloss *et al.*, 1977; Herman and Pollard, 1979), these were challenged based on technical considerations (e.g., Aubin *et al.*, 1979). Further, a study of mitotic cells using fluorescent phalloidin, a probe specific for F-actin, reported essentially no spindle labeling and yet robust labeling of the cortex

(Barak et al., 1981). Since that time, the failure to find mitotic spindle-associated F-actin has been repeated many times (with the exception of Fishkind and Wang, 1993), engendering a textbook view wherein F-actin is restricted to the periphery of mitotic cells (e.g., Karp, 2008).

Here we have reinvestigated the potential existence of spindle F-actin by developing improved methods for preservation of F-actin, by high-speed live-cell imaging, and by pharmacological disruption of F-actin. We find that in a vertebrate epithelium, F-actin is a consistent component of mitotic spindles that undergoes a characteristic series of changes in distribution and organization over the course of the cell cycle, that distinct pools of F-actin are associated with mitotic spindles, and that spindle-associated F-actin is mechanically coupled to the spindle itself.

RESULTS AND DISCUSSION
An extensive endoplasmic F-actin network in epithelial cells
GFP-UtrCH, an F-actin binding probe (Burkel et al., 2007) revealed cables of F-actin associated with mitotic spindles in Xenopus embryonic epithelial cells (Woolner et al., 2008). However, it is possible that rather than reflecting the distribution of endogenous F-actin these cables were a consequence of GFP-UtrCH-induced F-actin stabilization (e.g., Spracklen et al., 2014). Thus, we first sought to characterize endogenous F-actin in fixed samples. Standard F-actin staining approaches in which phalloidin was applied to samples well after fixation and washing resulted in intense staining of the cortex of Xenopus embryonic epithelial cells, but limited, disorganized F-actin staining of the endoplasm (Figure 1, A and A'), suggesting that endoplasmic F-actin is relatively labile (see also Schuh and Ellenberg, 2008). We therefore systematically modified the protocol with the goal of rapidly stabilizing F-actin during fixation. The protocol that produced the most consistent preservation of endoplasmic F-actin included fluorescent phalloidin and dimethyl sulfoxide (DMSO) in the fixative and imaging as soon after fixation as possible (the PDA—phalloidin, DMSO for actin—protocol; see Materials and Methods for details).

Analysis of PDA-fixed and optically cleared (see Materials and Methods) samples with laser scanning confocal microscopy revealed an extensive endoplasmic F-actin network, visible when the display is adjusted to the point where the cortex is saturated (Figure 1, B and B'). In interphase cells, F-actin is concentrated in the perinuclear region (Figure 1, B and E, solid arrowheads). It is also found in cables throughout the cytoplasm, some of which can extend from the nucleus to the cortex (Figure 1, B–E, empty arrowheads). In what are presumptively mitotic cells (based on the absence of a nucleus), F-actin cables are concentrated in structures that appear remarkably spindle-like, with a central region of loosely parallel cables flanked by two "poles" from which cables extend in a radial manner (Figure 1, B, B', and F–H, arrows). In addition, in both interphase and M-phase cells, F-actin is found in discrete cytoplasmic puncta (Figure 1, B–H). To determine whether the endoplasmic F-actin network was specific to Xenopus embryonic epithelia, we also applied the PDA fixative to zebrafish embryonic epithelia and human retinal pigmented epithelial (RPE) cells. Zebrafish epithelial cells showed extensive internal F-actin in both interphase and M-phase and in the latter the internal F-actin appeared to be spindle-associated based on comparison to chromatin (Figure 1I). Internal F-actin was also abundant in RPE cells (Figure 1J and Supplemental Figure 1, G, H, and H') although it was less obviously organized in a manner that resembled the spindle.

Spindle-associated F-actin and an F-actin cycle
To better characterize the organization of F-actin in Xenopus embryonic epithelia, F-actin distribution was compared with DNA and microtubules (Figure 2, A and B) or DNA alone (Figure 2C), which permitted faster sample processing and thus, slightly better preservation of endoplasmic F-actin. Consistent with the images above, a considerable amount of F-actin is associated with spindles (Figure 2, A–E). Moreover, the organization of this F-actin changes in a consistent manner during the cell cycle: In interphase, cables extend throughout the cytoplasm and puncta are apparently randomly distributed throughout the cell (Figure 2A). At the G2/M boundary, F-actin cables extend from the centrosomes toward the cortex and punctae appear to be more concentrated around the centrosomes (Figure 2, A, C, and E). In addition, F-actin cables are clearly evident running between the two nascent spindle poles. In prometaphase, the enrichment of punctae around the poles is more striking and the interpolar F-actin persists (Figure 2A, solid arrowheads). In metaphase, the cables running between the poles are lost while those running from the poles toward the cortex are maintained (Figure 2, A–E, empty arrowheads). In addition, in some samples, one or two particularly bright cables of F-actin were observed running from the cortex in the general region of the cell–cell junctions toward the poles or actually linking the cortex to the pole (Figure 2, B and C, arrows). In anaphase and telophase, interpolar F-actin cables reappeared and the punctae became more dispersed (Figure 2, A and C–E).

To ensure that the inclusion of phalloidin and DMSO in the fixative was not generating spindle-associated F-actin during fixation, two alternative approaches were employed, again with an emphasis on imaging as quickly as possible after fixation. First, samples fixed with paraformaldehyde and postextracted with methanol were stained with a directly labeled gamma actin antibody (Sonnemann et al., 2006). Although the endoplasmic F-actin did not appear to be as well preserved as it was in samples processed using the PDA protocol, spindle-associated F-actin cables and punctae were nonetheless evident (Figure 2D). Second, samples were fixed using cold acetone and, after washing, stained with phalloidin. Again, while the preservation of endoplasmic F-actin was inferior to that achieved with the PDA protocol, spindle-associated cables and punctae are nonetheless clearly evident (Figure 2E). Collectively, the above results show that endogenous F-actin forms an endoplasmic system that is far more extensive than is generally believed, which associates with the mitotic spindle in M-phase cells, and which undergoes reorganization at different stages of the cell cycle.

Visualization of spindle–F-actin in living cells
We next sought to characterize the dynamics of the spindle-associated F-actin in living embryos using swept-field confocal microscopy, which offers superior speed and sensitivity to that of our previous approach (Woolner et al., 2008; Davenport et al., 2016). Consistent with the results from fixed samples (see above) and from our previous study (Woolner et al., 2008) we found an extensive endoplasmic pool of F-actin (labeled with GFP-UtrCH) associated with the mitotic spindle (labeled with mCherry-α-tubulin; Figure 3A). Following metaphase onset, spindles in Xenopus embryonic epithelia undergo a stereotyped "dance" in which they slowly rotate and then display oscillatory motions before the onset of anaphase (Larson and Bement, 2017). We found that the meshwork of actin filaments moved in concert with the oscillating spindle, suggesting that the F-actin and microtubule arrays are mechanically coupled (Figure 3A' and Supplemental Movie 1). To test this possibility, we computed the optical flow field of microtubules and F-actin. This calculation revealed a mean correlation coefficient of 75% between the rotational components of the two flow fields (Figure 3, B and C; see Materials and Methods for details). This highly correlated
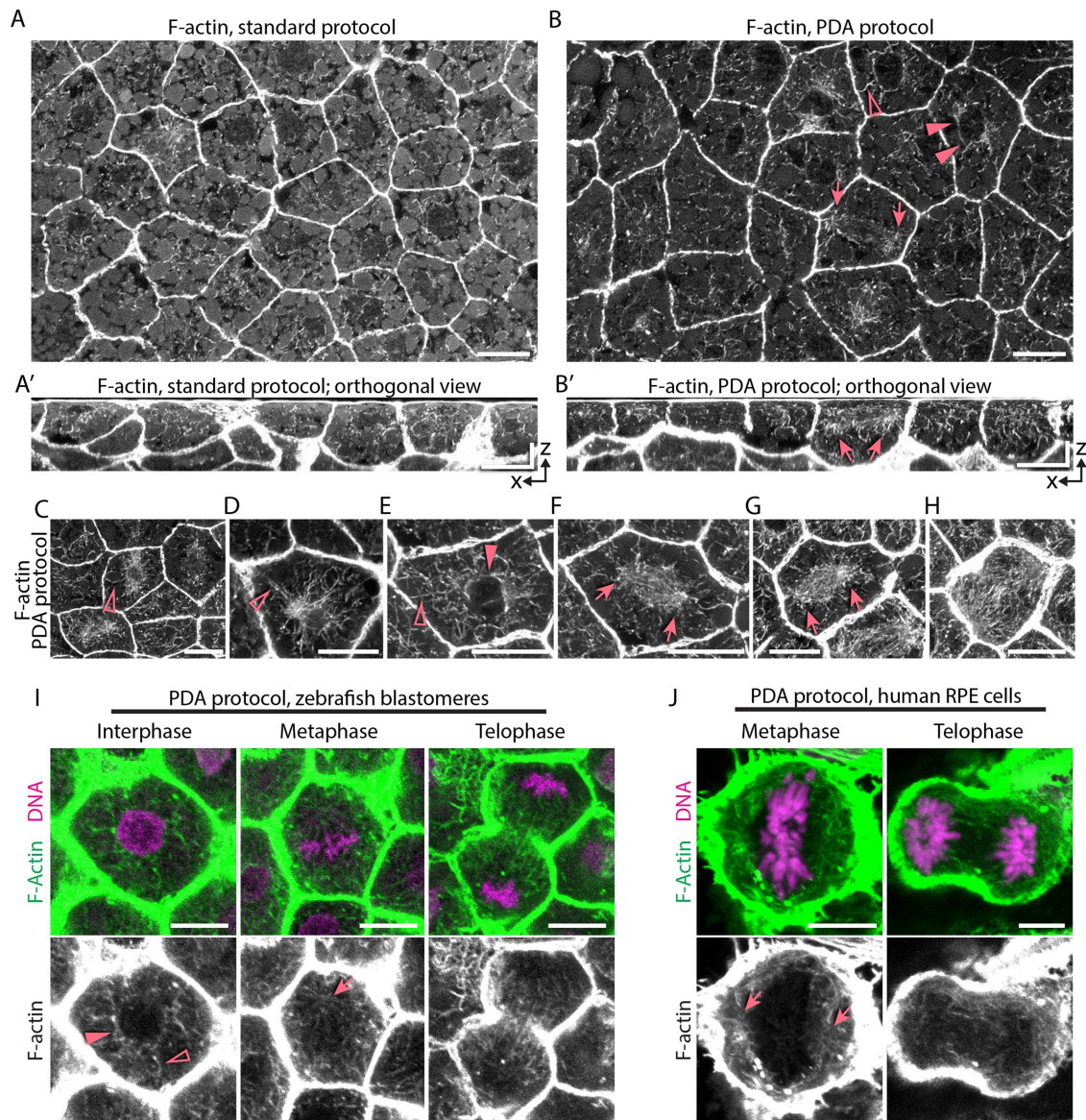
FIGURE 1: Comparison of fixation protocols for preservation of endoplasmic F-actin. (A) Sample stained with phalloidin after overnight washing. Cortical F-actin is abundant and internal F-actin is sparse and disorganized. (A') Orthogonal view of the epithelium in A. (B) PDA-fixed sample. Cortical and endoplasmic F-actin are abundant. F-actin cables extend from the nucleus (empty arrowhead), run parallel to the nucleus (solid arrowheads), and are organized in spindle-like structures (arrows). (B') Orthogonal view of epithelium shown in B; arrows point to the same structure seen in B. (C–H) PDA-fixed cells. (C) Mitotic cell with F-actin cable extending from a spindle-like structure toward cortex. (D) Interphase cell with F-actin cables emanating from one side of the nucleus. (E) Interphase cell with F-actin cables emanating from the nucleus. (F) Mitotic cell with F-actin cables organized in spindle shape. (G) Mitotic cell with F-actin cables organized in spindle shape. (H) Presumptive telophase cell with extensive endoplasmic F-actin cables. (I) Interphase, metaphase, and telophase zebrafish blastomeres fixed with the PDA protocol showing abundant endoplasmic F-actin; arrows and arrowheads mark apparently identical structures to those seen in B. (J) Metaphase and telophase RPE cells fixed with the PDA protocol showing abundant endoplasmic F-actin; arrows mark apparent spindle poles. Scale bars = 10 μm.

movement of F-actin and microtubules strongly suggests that the two structures are indeed mechanically coupled.

Targeting of F-actin cables from the cortex to the spindle poles

In addition to the endoplasmic meshwork of F-actin, we observed a pool of F-actin that closely resemble the cortex-to-spindle pole cables observed in fixed samples (Figure 2, B and C, arrows): Bright, finger-like cables that rapidly emanate from the cell cortex and

target the spindle (Figure 4A, arrowhead). In contrast to the endoplasmic spindle-associated F-actin network, which was found both apically and basally, the "fingers" appeared to arise predominantly from the junctional cortex. The fingers were specific to mitotic cells in that we never observed them in interphase cells (Supplemental Figure 1A). Plasma membrane markers failed to label the fingers (unpublished data) indicating that they are not derived from membrane evaginations emanating from neighboring cells (e.g., Negishi et al., 2016).
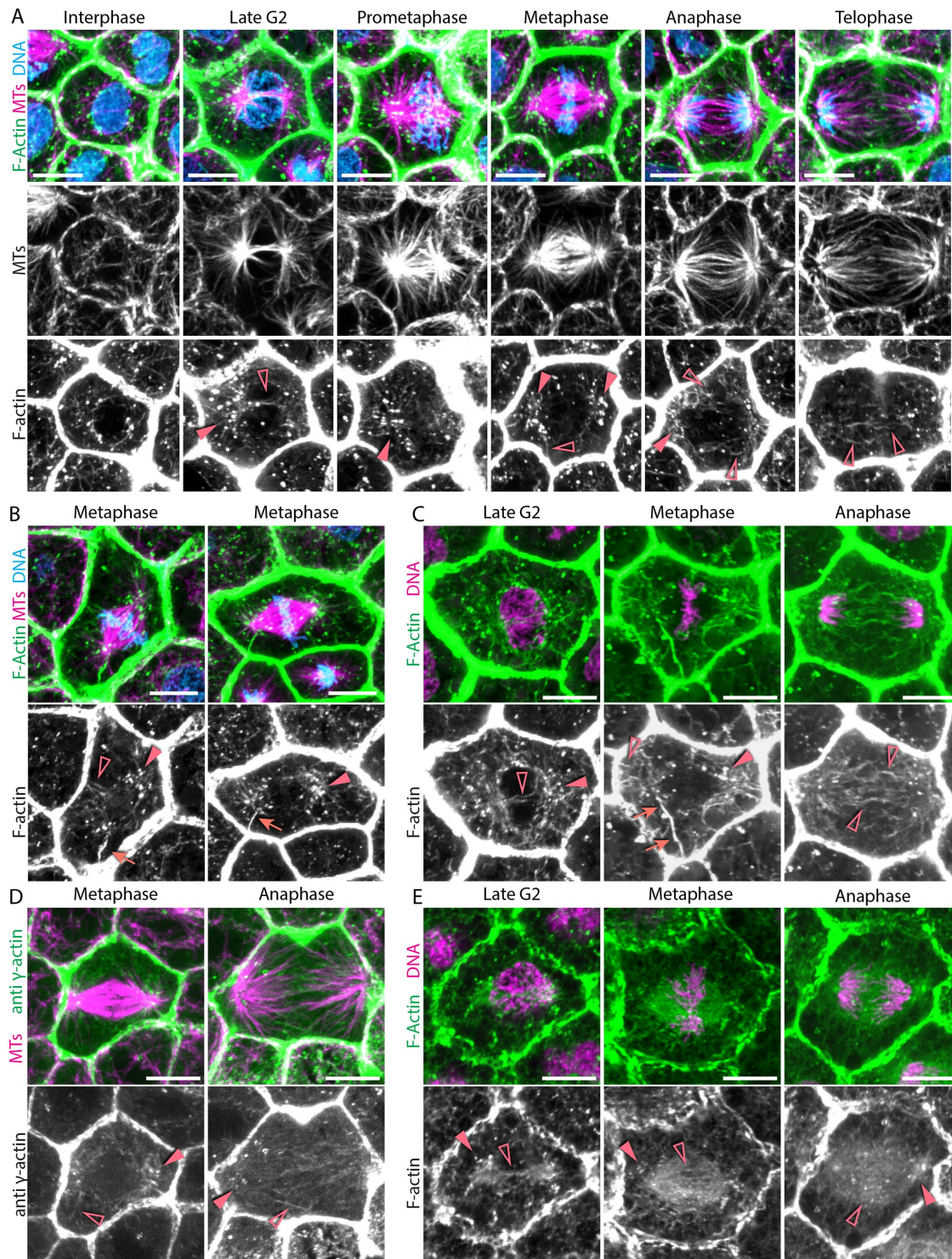
FIGURE 2: Mitotic spindle-associated F-actin in fixed samples. (A) PDA-fixed *X. laevis* epithelial cells labeled for DNA (mCherry-H2B, blue), microtubules (MTs; anti–α-tubulin, magenta), and F-actin (phalloidin, green). Clusters of F-actin punctae (solid arrowheads) are evident throughout the cell cycle as are F-actin cables (empty arrowheads). (B) Metaphase cells prepared as in A; F-actin punctae concentrate around spindle poles; bright F-actin cables run from the cortex toward the spindle poles (arrows). (C) PDA-fixed cells without anti-tubulin staining. In late G2 cables and punctae are abundant; in metaphase a long, bright cable (arrows) runs from the cortex toward the expected site of the spindle pole; in anaphase cables run between separating sister chromosomes. (D) Paraformaldehyde fixed, methanol extracted samples stained for microtubules (anti–α-tubulin, magenta) and actin (anti–γ-actin, green) have both spindle-associated F-actin cables and punctae. (E) Cold-acetone–fixed cells double labeled for DNA (mCherry-H2B, magenta), and F-actin (phalloidin, green) have spindle-associated F-actin cables and punctae. Scale bars = 10 μm.
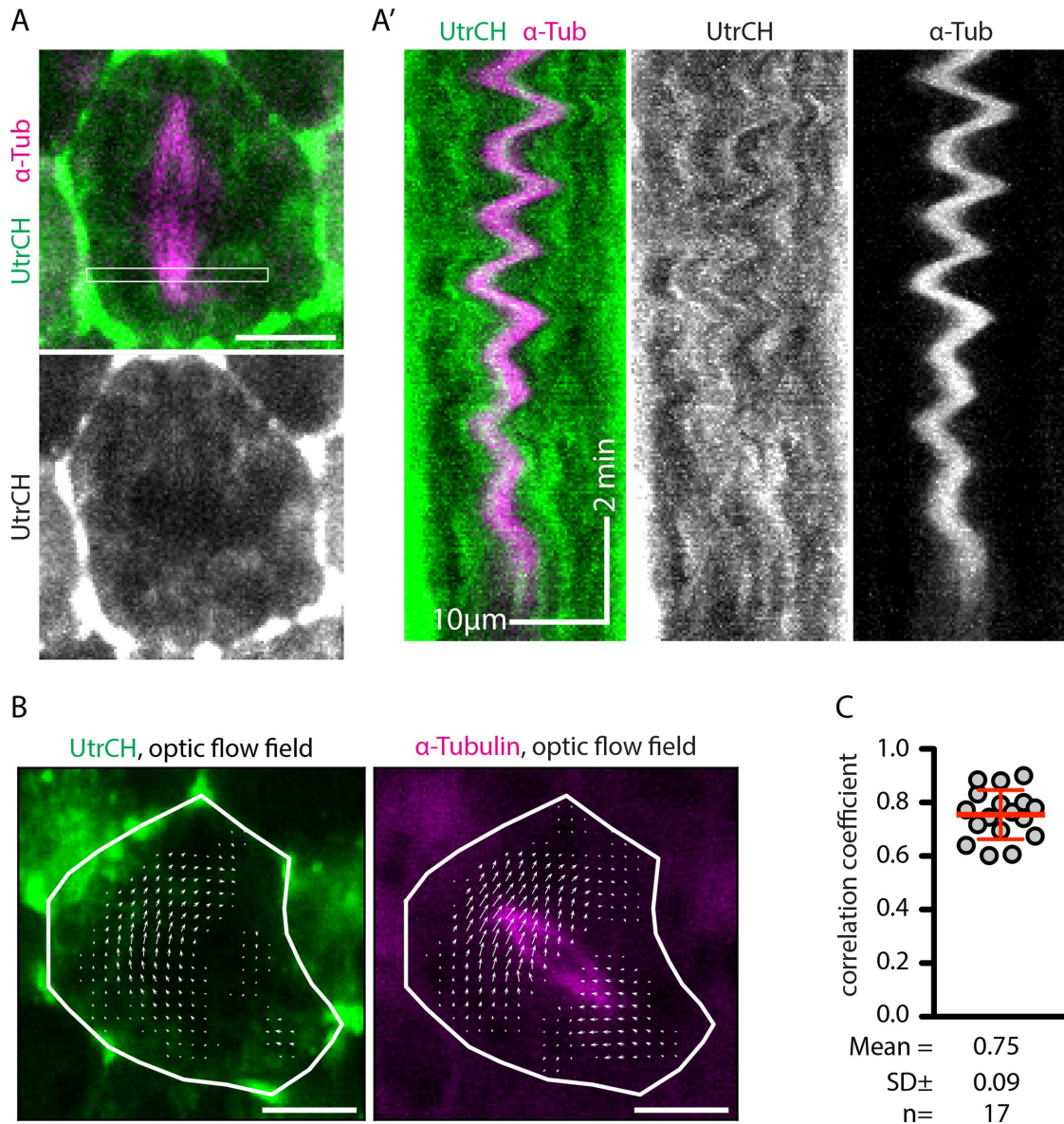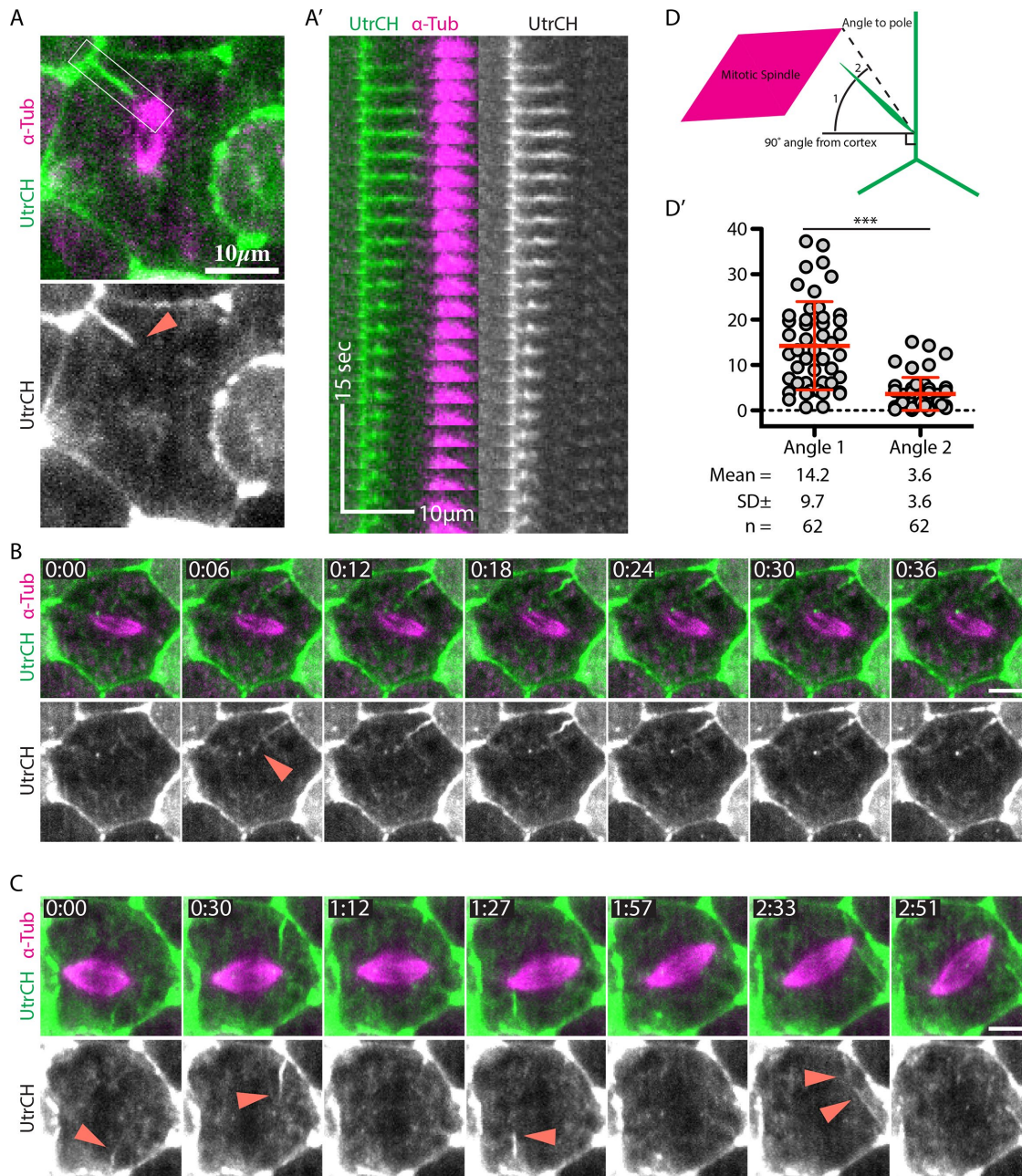
FIGURE 3: F-actin is coupled to the mitotic spindle. (A) Top, still image from a movie of live *X. laevis* epithelial cell expressing GFP-UtrCH (UtrCH, green) and mCh-α-tubulin (α-tub, magenta). Bottom, UtrCH alone. (A') Kymograph drawn from the white rectangle in A showing parallel oscillations of UtrCH and α-tubulin (see Supplemental Movie 1). (B) Still images from the sample prepared as in A; optical flow field for each probe overlaid on each image (white arrows). Horizontal scale bars = 10 μm; vertical scale bar = 2 min. (C) Scatter plot showing correlation coefficients for optical flow of GFP-UtrCH and mCh-α-tubulin. *N* = 17 cells from 12 different embryos; bars represent mean ± SD.

To better understand the fingers, we collected live imaging data from 40 mitotic cells from 16 different embryos expressing mCherry-α-tubulin and GFP-UtrCH. Of these 40 cells, 19 had one or more unambiguous actin "fingers." Most cells had one to two fingers, with a maximum of nine observed in one cell. Each targeting event consisted of an extremely rapid extension from the cell cortex (mean speed 0.93 ± 0.66 μm/s; maximum 4 μm/s) followed by a slow shrinkage back to its point of origin (Figure 4, A' and B; see also Supplemental Figure 1, B–F). The extension speed matches or exceeds extreme examples of formin-induced actin assembly achieved in vitro (Henty-Ridilla *et al.*, 2016) or via expression of constitutively active formins in vivo (Higashida *et al.*, 2004). The fingers are likely even more common than our measurements suggest because many cells were not imaged for all of mitosis and because their iden-

tification required that they be observed to both grow and shrink, thus, any fingers that extend only a short distance from the cortex to the pole could easily be missed.

The fingers were not only remarkable for their speed of extension, but also because they appeared to be specifically targeted to the spindle poles (Figure 4, A–C, arrowheads, and Supplemental Movie 2). To test this visual impression, we analyzed the relative differences in angles between each finger, a direct line to the spindle pole (Figure 4D, angle 2), and a line propagating at 90° from the cortex (Figure 4D, angle 1). We found that on average fingers deviated 14.2 ± 9.7° away from a 90° angle from the cortex, and only 3.6 ± 3.6° from a direct line to the spindle pole, indicating that the fingers nonrandomly target the spindle poles (Figure 4D').

FIGURE 4: Spindle pole–targeted F-actin fingers. (A) Top, still image from a movie of live *X. laevis* epithelial cell expressing GFP-UtrCH (UtrCH, green) and mCh-α-tubulin (α-tub, magenta). Bottom, UtrCH alone. Bright F-actin "finger" (arrowhead) extends from the cortex toward the spindle pole. (A') Vertical montage of 23 frames from the white rectangle in A showing the extension and retraction dynamics of a single F-actin finger (see Supplemental Movie 2). (B) Montage of the cell prepared as in A showing the dynamics of an F-actin finger (see Supplemental Movie 2). (C) Montage of the cell prepared as in A showing several F-actin fingers (see Supplemental Movie 2). Scale bars = 10 μm. Time in min:s. (D) Schematic representation of angles measured to determine the spindle pole targeting of F-actin fingers. (D') Scatterplot showing measured angles; *n* = 62 fingers from 40 different cells in 16 embryos; ***, *P* < 0.0001; bars represent mean ± SD.

Spindle actin and spindles are sensitive to a formin inhibitor

The cable organization of most of the endoplasmic F-actin suggested the involvement of formins. Accordingly, we assessed the effects of the formin inhibitor SMIFH2 (Rizvi *et al.*, 2009). SMIFH2 decreased endoplasmic F-actin while having no apparent effect on cortical F-actin (Figure 5, A and B). SMIF2 also produced two obvious spindle phenotypes: spindles were shorter (Figure 5, A and C), and mitosis was nearly twice as long (Figure 5, D and E). These results suggest that one or more formins nucleate the spindle-associated F-actin and that this F-actin is important for function. However, as in other studies where SMIFH2 has been shown to impact microtubules (e.g., Rosero *et al.*, 2013; Isogai *et al.*, 2015; Kim *et al.*, 2015), we cannot exclude the possibility that it impacts spindles not by way of F-actin loss, per se, but by inhibiting a potential interaction between microtubules and the formin FH2 domains (Roth-Johnson *et al.*, 2014) which serves as the target of SMIFH2 (Rizvi *et al.*, 2009) or by
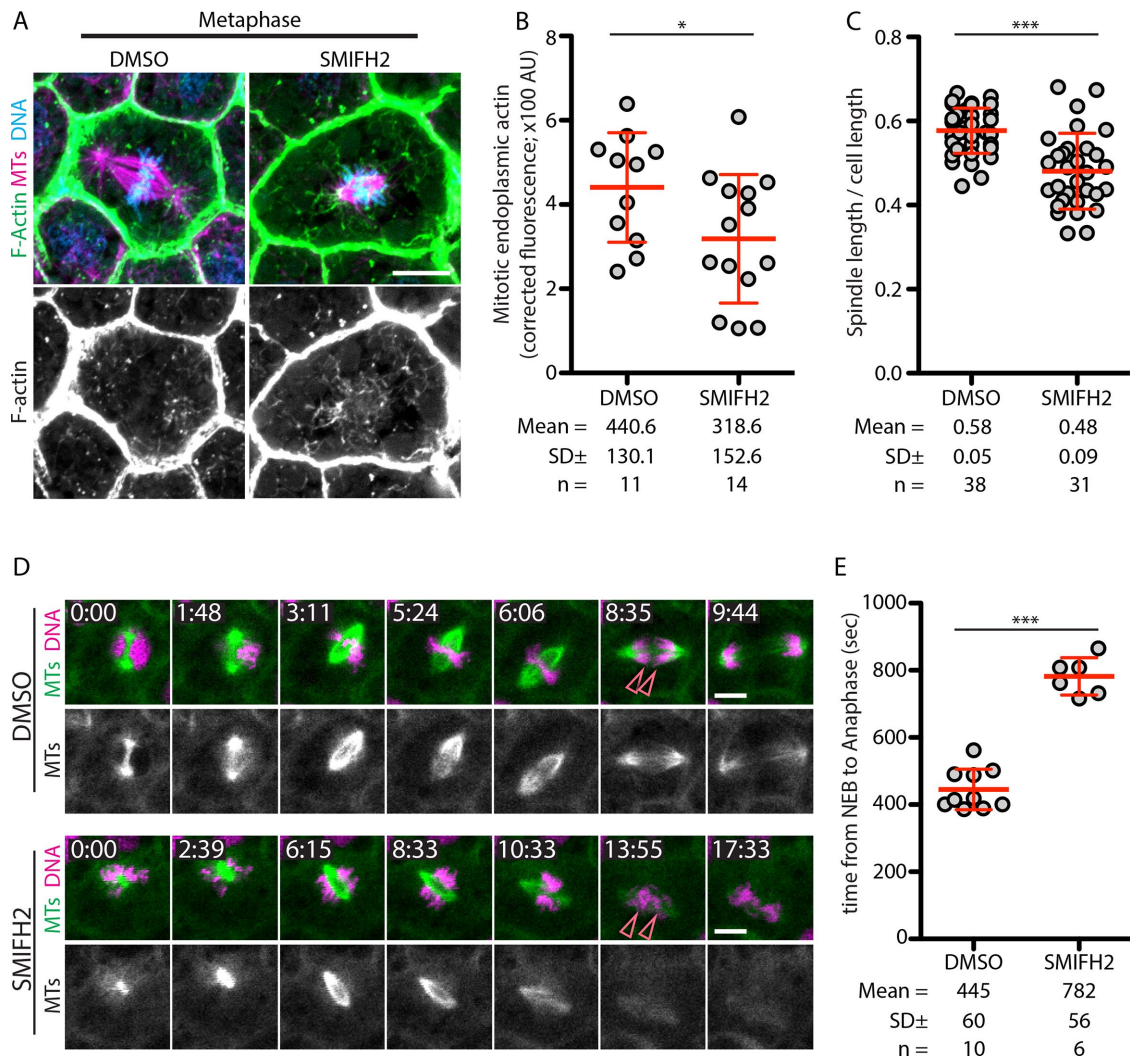
FIGURE 5: A formin inhibitor perturbs spindle F-actin, spindle length, and mitotic duration. (A) Images of PDA-fixed *X. laevis* epithelial cells labeled for DNA (mCherry-H2B, blue), microtubules (MTs; anti–α-tubulin, magenta), and F-actin (phalloidin, green) after treatment with SMIFH2 or DMSO. Scale bars = 10 μm. (B) SMIFH2-induced loss of spindle F-actin. Each dot represents a single cell (*n* = 11 cells from two DMSO-treated embryos and 14 cells from three SMIFH2-treated embryos), *, *P* = 0.045; bars represent mean ± SD. (C) SMIFH2-induced spindle shortening. *N* = 38 cells from nine DMSO-treated embryos and 31 cells from eight SMIFH2-treated embryos; ***, *P* < 0.0001; bars represent mean ± SD. (D) Images from a movie of *X. laevis* epithelial cells coexpressing GFP-α-tubulin (abbreviated MTs, green) and mCh-H2B (DNA, magenta) and treated either with SMIFH2 or DMSO. Empty arrowheads mark the location of the separating anaphase chromosomes. Scale bars = 10 μm. Time is in min:s. (E) SMIFH2-induced lengthening of mitosis as measured from nuclear envelope breakdown to anaphase (*n* = 10 cells from six DMSO-treated embryos and six cells from four SMIFH2-treated embryos); ***, *P* < 0.0001; bars represent mean ± SD.

impairing the interaction of profilin with microtubules (Nejedla *et al.*, 2016), in that profilin has been shown to directly promote microtubule assembly (Henty-Ridilla *et al.*, 2017).

The following simple, but important points emerge from this study: First, the endoplasmic pool of F-actin is far more extensive than is generally recognized, not only for M-phase cells, but also for interphase cells. These results add to a growing body of evidence for internal F-actin playing roles in a variety of noncortical locations including centrosomes (e.g., Sider *et al.*, 1999; Obino *et al.*, 2016; Inoue *et al.*, 2019), the nucleus (reviewed in Plessner and Grosse, 2019), on mitochondria (e.g., Korobova *et al.*, 2013), and on the endoplasmic reticulum (Chakrabarti *et al.*, 2018). Second, endoplasmic F-actin is labile in fixed samples, which likely explains why it has been overlooked. Third, the spindle

associates with three different pools of F-actin: punctae, relatively stable cables that move in concert with the spindle, and highly dynamic cables that shoot from the cortex toward the spindle poles and then recoil. Although it could be argued that the results obtained here reflect a special feature of *Xenopus* epithelial cells, given our findings with zebrafish epithelial cell spindles and human RPE spindles, we suspect that spindle actin is the norm. Consistent with this possibility, a recent study reported that an Arp2/3-dependent pool of F-actin develops at mitotic spindle poles upon mitotic exit in HeLa cells (Farina *et al.*, 2019). Perhaps most tellingly, F-actin is associated with and/or plays important roles in mitotic spindles in plants (e.g., Forer *et al.*, 1979; Seagull *et al.*, 1987; Yu *et al.*, 2006) and meiotic spindles in animals (e.g., Silverman-Gavrila and Forer, 2000; Weber *et al.*, 2004;

Azoury *et al.*, 2008; Schuh and Ellenberg, 2008; Mogessie and Schuh, 2017; Burdyniuk *et al.*, 2018).

What does the spindle-associated F-actin described in this study do? The cross-correlational analysis demonstrates that the relatively stable F-actin is physically coupled to the spindle, which means that at a minimum it influences the stereotyped metaphase spindle dance (Larson and Bement, 2017). Because completion of the dance occurs as the spindle reaches the approximate center of the cell (in X and Y) it follows that the relatively stable F-actin network may be involved in spindle positioning.

The F-actin fingers, which, based on their staining intensity we assume represent cables rather than single filaments, are particularly provocative. Their speed and remarkable ability to selectively target spindle poles suggests a scenario in which contact of a spindle pole microtubule with the cortex stimulates formin-dependent actin polymerization (Martin *et al.*, 2005), possibly via interaction of a plus tip protein with a cortical formin (Henty-Ridilla *et al.*, 2016). However, for such a mechanism to result in pole targeting, the resultant cables would need the means to maintain rapid growth while tracking along the microtubule. The roles, if any, played by the fingers are even more mysterious. However, because it was previously proposed that communication between the spindle poles and cortex is involved in the metaphase–anaphase transition in these cells (Larson and Bement, 2017; Sandquist, Larson *et al.*, 2018), we are attracted to the possibility that the F-actin fingers may represent a conduit for exchange of cell cycle control proteins between the spindle and the cortex.

MATERIALS AND METHODS
Embryo preparation and drug treatments
Adult *Xenopus laevis* females were injected with 800 U of human chorionic gonadotropin (HCG; MP Biomedicals) into the dorsal lymph sac 12–18 h before use. Eggs were laid into 1X Marc's Modified Ringer's (MMR; 100 mM NaCl, 2 mM KCl, 1 mM MgCl$_2$, and 5 mM HEPES, pH 7.4) and fertilized in vitro with macerated testes. Embryos were dejellied in 2% cysteine solution (in 0.1X MMR, pH 7.8) and then rinsed five times in 1X MMR and five times in 0.1X MMR. Embryos processed for fixation and immunofluorescence were cultured overnight at 16°C in 0.1X MMR. Embryos used for live imaging were either cultured overnight at 16°C (Figure 5D) or for 3 d at 14°C (Figures 3 and 4). SMIFH2 treatments were performed at 20 µM in 0.1X MMR for 30 min before fixation or live imaging. Controls were incubated in an equivalent concentration of DMSO in 0.1X MMR for the same amount of time.

mRNA preparation and embryo microinjection
The mCherry-histone H2B, mCherry-α-tubulin, eGFP-α-tubulin, and eGFP-UtrCH plasmids were made as previously described (Burkel *et al.* 2007; Miller and Bement 2009).

All mRNA was transcribed in vitro using the mMessage Machine SP6 kit (Life Technologies) and reactions were purified with the RNeasy Mini Kit (Qiagen). Embryos were submerged in 0.1X MMR + 5% Ficoll (Sigma) and injected with an 8 nl volume at the two-cell stage. mCherry-histone H2B was injected at 12.5 µg/ml for both live- and fixed-cell imaging. For live-cell imaging, GFP- and mCherry-α-tubulin was injected at 13.5 µg/ml, and GFP-UtrCH was injected at 20 µg/ml.

Fixation and immunofluorescence
To fix for double labeling of F-actin and microtubules, *Xenopus* embryos were briefly rinsed in 1X phosphate-buffered saline (PBS), and then dropped into a modified paraformaldehyde (PFA) solution (the

PDA protocol). For 10 ml of the PDA fix, we combined the following: 7.75 ml "superfix" buffer (100 mM KCl, 3 mM MgCl, 10 mM HEPES, 150 mM sucrose, pH 7.4), 1 ml fresh 37% formaldehyde, 1 ml DMSO, 200 µl 100 mM ethylene glycol-bis(β-aminoethylether)-*N*,*N*,*N′*,*N′*-tetraacetic acid (EGTA), 10 µl 50% glutaraldehyde, 1 µl 2 mM Taxol. Addition of Taxol to fix for microtubule preservation was previously described by Gard (1991) who showed that at concentrations below 500 nM (final) Taxol helps preserve preexisting microtubules without promoting new microtubule assembly. Fluorescent phalloidin (Alexa Flour 488; Life Technologies), desiccated and rehydrated in PBS to remove methanol, was added to the fix buffer at a final concentration of 2 U/ml, and supplemented to primary and secondary antibody incubations at 1 U/ml for next day imaging. Embryos were incubated for 1 h on an orbital shaker at room temperature to fix. Microtubules were labeled using mouse monoclonal anti–α-tubulin (DM1A; Sigma) at 1:20,000 and a donkey derived anti-mouse secondary was used at 1:10,000 (AlexaFluor 647; Life Technologies). Primary antibody incubations were 3 h at room temperature while secondary incubations were overnight at 4°C.

Zebrafish embryos were incubated for 6–7 h after fertilization and fixed for 3 h with PDA fix containing Alexa 546 phalloidin to allow visualization of genetically encoded GFP. Zebrafish embryos were also stained with 10 nM To-Pro-3 iodide to label DNA. Human RPE cells were grown on #1.5 glass coverslips and fixed for 30 min at room temperature with PDA fix containing BODIPY-FL phallacidin. RPE cells were also stained postfix with 1 µg/ml DAPI and 1 U/ml BODIPY-FL phallacidin.

For cold-acetone fixation, *Xenopus* embryos were rinsed in 1X PBS and then dropped directly into acetone chilled to –20°C. Embryos were incubated for 20 min in acetone at –20°C and then rehydrated in acetone:PBS serial washes. To label F-actin, embryos were blocked in 1X PBST + 0.1% bovine serum albumin (BSA; Sigma) for 10 m, then incubated in 1X PBST + 0.1% BSA with 1:200 fluorescent phalloidin for 30 min, followed by brief washes with 1X PBS alone.

Actin antibody experiments were performed using a modified version of the microtubule fixation protocol in Danilchik *et al.* (1998). *Xenopus* embryos were fixed for 1 h in 3.7% PFA, 0.25% glutaraldehyde, and 0.2% Triton X-100 in a microtubule assembly buffer (80 mM K-PIPES, pH 6.8, 5 mM EGTA, 1 mM MgCl$_2$, pH 7.4). Following fixation, embryos were postfixed in –20°C methanol for 30 min and then rehydrated with a methanol:PBS wash series. Samples were incubated for 3 h at room temperature with 1:100 mouse monoclonal anti–γ-actin 1-37::488 (a gift from James Ervasti, University of Minnesota).

Following all fixation techniques, *Xenopus* embryos were dehydrated using a series of isopropanol in PBS washes and then cleared with Murray's Clear (2:1 benzyl alcohol, benzyl benzoate) for confocal microscopy. Zebrafish embryos and RPE cells were mounted in 70% glycerol in PBS for imaging.

Microscopy and image processing
Imaging of all fixed experiments was conducted either with a CFI Plan Apo 60X/1.4 NA oil immersion objective (Nikon) using a Prairie View laser scanning confocal (Bruker) on a Nikon Eclipse Ti inverted microscope (Figures 1, A–H, 2, and 5) or with a PlanApo N 60X/1.42 NA oil immersion objective using an Olympus Fluoview 1000 laser scanning confocal. Z-series were acquired using 0.5 µm step size (Bruker) or 0.2 µm step size (Olympus). All images of fixed cells are maximum-intensity projections 2–10 µm thick through the middle of the cell. For live imaging in Figure 5, embryos were mounted in 0.1X MMR and imaged using a CFI Plan Apo 40X/1.0 NA oil immersion objective on the Bruker confocal described

above, acquiring a single optical plane every 2.3 s. For the live imaging in Figures 3 and 4, embryos were mounted in 0.1X MMR and imaged using a CFI Plan Apo 60X/1.4 NA oil immersion objective on a Nikon Eclipse Ti inverted microscope equipped with an Opterra swept-field confocal unit (Bruker), a PZ-2000FT series piezo XYZ stage (ASI), and an Evolve Delta EMCCD camera (Photometrics). Both Nikon microscopes were controlled, and images acquired using Prairie View software (Bruker). All images of live cells in Figures 3 and 4 are maximum-intensity projections of three 0.8-μm slices acquired every 3 s. Image processing of fixed images was limited to maximum-intensity projection in Fiji (Schindelin et al., 2012) and contrast adjustment to best display spindle-associated F-actin, with the exception of Figure 1J, which was processed to correct for spectral bleedthrough of DAPI fluorescence into the BODIPY-FL channel. Live time series were maximum-intensity projected in Fiji, registered for two-dimensional (2D) drift using the StackReg plug-in (Thévenaz et al., 1998), and corrected for bleaching using an exponential fit within Fiji. The kymograph in Figure 3A′ was generated by reslicing a rectangle 83 × 10 pixels in size and then max projecting the resulting stack. Where it was necessary to rotate images, they were rotated only once and bicubic interpolation was used. Image LUTs were assigned using Fiji, and figures were assembled using Adobe Illustrator.

Image quantification

Mitotic endoplasmic actin fluorescence was calculated for individual cells by subtracting the average background intensity from the average endoplasmic actin intensity. Optic flows for actin and tubulin fluorescence were measured using the FlowJ plug-in (Abràmoff et al., 2000) with the following parameters: "Lucas and Kanade algorithm," $\Sigma_s = 1.5$, $\Sigma_t = 1.0$, $\Sigma_w = 5.0$, $\tau = 1.0$. Then we compensated the translation and rotation of the cell as a whole. To achieve this, we approximated the 2D cross-section of a cell by a polygon and manually tracked the position of its n vertices $\overline{r}_\alpha$. By discrete differentiation we obtained vertex velocities $\overline{v}_i$. We calculated vertex weights as follows:

$$w_\alpha = \frac{A_{\alpha-1,\alpha} + A_{\alpha,\alpha+1}}{2A}$$

where $A_{i,j}$ is the area of triangle with vertices $\overline{r}_i, \overline{r}_j, \overline{r}_c$ ($\overline{r}_c$ is the position of the centroid) and A is the area of the cell polygon. The translational and rotational velocities were estimated as follows:

$$\begin{pmatrix} u_c \\ v_c \end{pmatrix} = \sum_\alpha w_\alpha \overline{v}_\alpha, \quad \omega = \sum_\alpha \frac{w_\alpha (\overline{r}_\alpha \times \overline{v}_\alpha)}{|\overline{r}_\alpha|^2}$$

where $\overline{a} \times \overline{b} = a_x b_y - a_y b_x$. Finally, flows were compensated as follows:

$$u'_i = u_i - u_c + \omega y_i, \quad v'_i = v_i - v_c - \omega x_i$$

where x_i, y_i are the coordinates of the ith pixel and u_i, v_i are the x and y flow components.

We then calculated the rotational component V of the flow as follows:

$$V = \frac{1}{A} \sum_i \left((x_i - x_c) v'_i - (y_i - y_c) u'_i \right)$$

where summation is taken over all pixels of the cell. Finally, we considered rotational components of actin and tubulin channels V_a and V_t for all frames and calculated the Pearson correlation coefficient for the whole image sequence:

$$r = \frac{cov(V_a, V_t)}{\sigma_{V_a} \sigma_{V_t}}$$

Statistical tests

The P values in Figure 5 are from a two-sided, unpaired t test (Figure 5, B and E) with Welch's correction for unequal variance (Figure 5C). The P value in Figure 5D′ is from a two-sided, paired t test.

Note added in proof. After this paper was accepted a study was published describing spindle-associated F-actin in cultured human and mouse cells (Plessner et al., 2019).

REFERENCES
Abràmoff MD, Niessen WJ, Viergever MA (2000). Objective quantification of the motion of soft tissues: an application to orbital soft tissue motion. IEEE Trans Med Imag 19, 986–995.

Aubin JE, Weber K, Osborn M (1979). Analysis of actin and microfilament-associated proteins in the mitotic spindle and cleavage furrow of PtK2 cells by immunofluorescence microscopy. A critical note. Exp Cell Res 124, 93–109.

Azoury J, Lee KW, Georget V, Rassinier P, Leader B, Verlhac MH (2008). Spindle positioning in mouse oocytes relies on a dynamic meshwork of actin filaments. Curr Biol 18, 1514–1519.

Barak LS, Nothnagel EA, DeMarco EF, Webb WW (1981). Differential staining of actin in metaphase spindles with 7-nitrobenz-2-oxa-1,3-diazole-phallacidin and fluorescent DNase: is actin involved in chromosomal movement? Proc Natl Acad Sci USA 78, 3034–3038.

Burdyniuk M, Callegari A, Mori M, Nédélec F, Lénárt P (2018). F-actin nucleated on chromosomes coordinates their capture by microtubules in oocyte meiosis. J Cell Biol 217, 2661–2674.

Burkel BM, von Dassow G, Bement WM (2007). Versatile fluorescent probes for actin filaments based on the actin-binding domain of utrophin. Cell Motil Cytoskeleton 64, 822–832.

Cande WZ, Lazarides E, McIntosh JR (1977). A comparison of the distribution of actin and tubulin in the mammalian mitotic spindle as seen by indirect immunofluorescence. J Cell Biol 72, 552–567.

Chakrabarti R, Ji WK, Stan RV, de Juan Sanz J, Ryan TA, Higgs, HN (2018). INF2-mediated actin polymerization at the ER stimulates mitochondrial calcium uptake, inner membrane constriction, and division. J Cell Biol 217, 251–268.

Danilchik MV, Funk WC, Brown EE, Larkin K (1998). Requirement for microtubules in new membrane formation during cytokinesis of Xenopus embryos. Dev Biol 194, 47–60.

Davenport NR, Sonnemann KJ, Eliceiri KW, Bement WM (2016). Membrane dynamics during cellular wound repair. Mol Biol Cell 27, 2272–2285.

Farina F, Gaillard J, Guérin C, Couté Y, Sillibourne J, Blanchoin L, Théry M (2016). The centrosome is an actin-organizing centre. Nat Cell Biol 18, 65–75.

Farina F, Ramkumar N, Brown L, Samandar Eweis D, Anstatt J, Waring T, Bithell J, Scita G, Théry M, Blanchoin M, et al. (2019). Local actin nucleation tunes centrosomal microtubule nucleation during passage through mitosis. EMBO J 38, e99843.

Fishkind DJ, Wang YL (1993). Orientation and three-dimensional organization of actin filaments in dividing cultured cells. J Cell Biol 123, 837–848.

Forer A, Jackson WT, Engberg A. (1979). Actin in spindles of *Haemanthus katherinae* endosperm. II. Distribution of actin in chromosomal spindle fibres, determined by analysis of serial sections. J Cell Sci 37, 349–371.

Gard DL (1991). Organization, nucleation, and acetylation of microtubules in *Xenopus laevis* oocytes: a study by confocal immunofluorescence microscopy. Dev Biol 143, 346–362.

Gawadi N (1971). Actin in the mitotic spindle. Nature 234, 410.

Henty-Ridilla JL, Rankova A, Eskin JA, Kenny K, Goode BL (2016). Accelerated actin filament polymerization from microtubule plus ends. Science 352, 1004–1009.

Henty-Ridilla JL, Juanes MA, Goode BL (2017). Profilin directly promotes microtubule growth through residues mutated in amyotrophic lateral sclerosis. Curr Biol 27, 3535–3543

Herman IM, Pollard TD (1979). Comparison of purified anti-actin and fluorescent-heavy meromyosin staining patterns in dividing cells. J Cell Biol 80, 509–520.

Higashida C, Miyoshi T, Fujita A, Oceguera-Yanez F, Monypenny J, Andou Y, Narumiya S, Watanabe N (2004). Actin polymerization-driven molecular movement of mDia1 in living cells. Science 303, 2007–2010.

Inoue D, Obino D, Farina F, Gaillard J, Guerin C, Blanchoin L, Lennon-Duménil AM, Théry M (2019). Actin filaments regulate microtubule growth at the centrosome. EMBO J, doi: 10.15252/embj.201899630.

Isogai T, van der Kammen R, Innocenti M (2015). SMIFH2 has effects on Formins and p53 that perturb the cell cytoskeleton. Sci Rep 5, 9802.

Karp G (2008). Cell and molecular biology. In: Concepts and Experiments, 5th ed., New York: John Wiley & Sons, 328–329.

Kim HC, Jo YJ, Kim NH, Namgoong S (2015). Small molecule inhibitor of formin homology 2 domains (SMIFH2) reveals the roles of the formin family of proteins in spindle assembly and asymmetric division in mouse oocytes. PLoS One 10, e0123438.

Kimura H, Miki Y, Nakanishi A (2014). Centrosomes at M phase act as a scaffold for the accumulation of intracellular ubiquitinated proteins. Cell Cycle 13, 1928–1937.

Korobova F, Ramabhadran V, Higgs HN (2013). An actin-dependent step in mitochondrial fission mediated by the ER-associated formin INF2. Science 339, 464–467.

Larson ME, Bement WM (2017). Automated mitotic spindle tracking suggests a link between spindle dynamics, spindle orientation, and anaphase onset in epithelial cells. Mol Biol Cell 28, 746–759.

Loughlin R, Wilbur JD, McNally FJ, Nédélec FJ, Heald R (2011). Katanin contributes to interspecies spindle length scaling in *Xenopus*. Cell 147, 1397–1407.

Magidson V, Paul R, Yang N, Ault JG, O'Connell CB, Tikhonenko I, McEwen BF, Mogilner A, Khodjakov A (2015). Adaptive changes in the kinetochore architecture facilitate proper spindle assembly. Nat Cell Biol 17, 1134–1144.

Martin SG, McDonald WH, Yates JR 3rd, Chang F (2005). Tea4p links microtubule plus ends with the formin for3p in the establishment of cell polarity. Dev Cell 8, 479–491.

Miller AL, Bement WM (2009). Regulation of cytokinesis by Rho GTPase flux. Nat Cell Biol 11, 71–77.

Mogessie B, Schuh M (2017). Actin protects mammalian eggs against chromosome segregation errors. Science 357, eaal1647.

Negishi T, Miyazaki N, Murata K, Yasuo H, Ueno N (2016). Physical association between a novel plasma membrane structure and centrosome orients cell division. Elife 5, e16550.

Nejedla M, Sadi S, Sulimenko V, de Almeida FN, Blom H, Draber P, Aspenström P, Karlsson R (2016). Profilin connects actin assembly with microtubule dynamics. Mol Biol Cell 27, 2381–2393.

Nousiainen M, Silljé HH, Sauer G, Nigg EA, Körner R (2006). Phosphoproteome analysis of the human mitotic spindle. Proc Natl Acad Sci USA 103, 5391–5396.

Obino D, Farina F, Malbec O, Sáez PJ, Maurin M, Gaillard J, Dingli F, Loew D, Gautreau A, Yuseff MI, *et al.* (2016). Actin nucleation at the centrosome controls lymphocyte polarity. Nat Commun 7, 10969.

Plessner M, Grosse R (2019). Dynamizing nuclear actin filaments. Curr Opin Cell Biol 56, 1–6.

Plessner M, Knerr J, Grosse R (2019). Centrosomal actin assembly is required for proper mitotic spindle formation and chromosome congression. iScience 15, 274–281.

Rizvi SA, Neidt EM, Cui J, Feiger Z, Skau CT, Gardel ML, Kozmin SA, Kovar DR (2009). Identification and characterization of a small molecule inhibitor of formin-mediated actin assembly. Chem Biol 16, 1158–1168.

Rosenblatt J, Cramer LP, Baum B, McGee KM (2004). Myosin II-dependent cortical movement is required for centrosome separation and positioning during mitotic spindle assembly. Cell 117, 361–372.

Rosero A, Žárský V, Cvrčková F (2013). AtFH1 formin mutation affects actin filament and microtubule dynamics in *Arabidopsis thaliana*. J Exp Bot 64, 585–597.

Roth-Johnson EA, Vizcarra CL, Bois JS, Quinlan ME (2014). Interaction between microtubules and the *Drosophila* formin Cappuccino and its effect on actin assembly. J Biol Chem 289, 4395–4404.

Sandquist JC, Kita AM, Bement WM (2011). And the dead shall rise: actin and myosin return to the spindle. Dev Cell 21, 410–419.

Sandquist JC, Larson ME, Woolner S, Ding Z, Bement WM (2018). An interaction between myosin-10 and the cell cycle regulator Wee1 links spindle dynamics to mitotic progression in epithelia. J Cell Biol 217, 849–859.

Sanger JW (1975). Presence of actin during chromosomal movement. Proc Natl Acad Sci USA 72, 2451–2455.

Schindelin J, Arganda-Carreras I, Frise E, Kaynig V, Longair M, Pietzsch T, Preibisch S, Rueden C, Saalfeld S, Schmid B, *et al.* (2012). Fiji: an open-source platform for biological-image analysis. Nat Methods 9, 676–682.

Schloss JA, Milsted A, Goldman RD (1977). Myosin subfragment binding for the localization of actin-like microfilaments in cultured cells. A light and electron microscope study. J Cell Biol 74, 794–815.

Schuh M, Ellenberg J (2008). A new model for asymmetric spindle positioning in mouse oocytes. Curr Biol 18, 1986–1992.

Seagull RW, Falconer MM, Weerdenburg CA (1987). Microfilaments: dynamic arrays in higher plant cells. J Cell Biol 104, 995–1004.

Sider JR, Mandato CA, Weber KL, Zandy AJ, Beach D, Finst RJ, Skoble J, Bement WM (1999). Direct observation of microtubule-f-actin interaction in cell free lysates. J Cell Sci 112, 1947–1956.

Silverman-Gavrila RV, Forer A (2000). Evidence that actin and myosin are involved in the poleward flux of tubulin in metaphase kinetochore microtubules of crane-fly spermatocytes. J Cell Sci 113, 597–609.

Skop AR, Liu H, Yates J 3rd, Meyer BJ, Heald R (2004). Dissection of the mammalian midbody proteome reveals conserved cytokinesis mechanisms. Science 305, 61–66.

Sonnemann KJ, Fitzsimons DP, Patel JR, Liu Y, Schneider MF, Moss RL, Ervasti JM (2006). Cytoplasmic γ-actin is not required for skeletal muscle development but its absence leads to a progressive myopathy. Dev Cell 11, 387–397.

Spracklen AJ, Fagan TN, Lovander KE, Tootle TL (2014). The pros and cons of common actin labeling tools for visualizing actin dynamics during *Drosophila* oogenesis. Dev Biol 393, 209–226.

Théry M, Racine V, Pépin A, Piel M, Chen Y, Sibarita JB, Bornens M (2005). The extracellular matrix guides the orientation of the cell division axis. Nat Cell Biol 7, 947–953.

Thévenaz P, Ruttimann UE, Unser M (1998). A pyramid approach to subpixel registration based on intensity. IEEE Trans Image Process 7, 27–41.

Toyoshima F, Nishida E (2007). Integrin-mediated adhesion orients the spindle parallel to the substratum in an EB1- and myosin X-dependent manner. EMBO J 26, 1487–1498.

Weber KL, Sokac AM, Berg JS, Cheney RE, Bement WM (2004). A microtubule-binding myosin required for nuclear anchoring and spindle assembly. Nature 431, 325–329.

Woolner S, O'Brien LL, Wiese C, Bement WM (2008). Myosin-10 and actin filaments are essential for mitotic spindle function. J Cell Biol 182, 77–88.

Yu M, Yuan M, Ren H (2006). Visualization of actin cytoskeletal dynamics during the cell cycle in tobacco (*Nicotiana tabacum* L. cv Bright Yellow) cells. Biol Cell 98, 295–306.